Mapping the Seismicity of Mars With InSight

S. Ceylan, D. Giardini, J. F. Clinton, D. Kim, A. Khan, S. C. Stähler, G. Zenhäusern, P. Lognonné, W. B. Banerdt

▶ **To cite this version:**

S. Ceylan, D. Giardini, J. F. Clinton, D. Kim, A. Khan, et al.. Mapping the Seismicity of Mars With InSight. Journal of Geophysical Research. Planets, 2023, 128, ⟨10.1029/2023JE007826⟩. ⟨insu-04199335⟩

HAL Id: insu-04199335

https://insu.hal.science/insu-04199335v1

Submitted on 7 Sep 2023

HAL is a multi-disciplinary open access archive for the deposit and dissemination of scientific research documents, whether they are published or not. The documents may come from teaching and research institutions in France or abroad, or from public or private research centers.

L'archive ouverte pluridisciplinaire **HAL**, est destinée au dépôt et à la diffusion de documents scientifiques de niveau recherche, publiés ou non, émanant des établissements d'enseignement et de recherche français ou étrangers, des laboratoires publics ou privés.

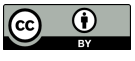

Distributed under a Creative Commons CC BY 4.0 - Attribution - International License

Check for updates

JGR Planets

RESEARCH ARTICLE
10.1029/2023JE007826

Special Section:
The Large Marsquake of Sol 1222

Mapping the Seismicity of Mars With InSight

S. Ceylan[1], D. Giardini[1], J. F. Clinton[2], D. Kim[1], A. Khan[1,3], S. C. Stähler[1,4], G. Zenhäusern[1], P. Lognonné[5], and W. B. Banerdt[6]

[1]Institute of Geophysics, ETH Zurich, Zurich, Switzerland, [2]Swiss Seismological Service, ETH Zurich, Zurich, Switzerland, [3]Institute of Geochemistry and Petrology, ETH Zurich, Zurich, Switzerland, [4]Physik-Institut, University of Zurich, Zurich, Switzerland, [5]Université Paris Cité, Institut de Physique du Globe de Paris, CNRS, Paris, France, [6]Jet Propulsion Laboratory, California Institute of Technology, Pasadena, CA, USA

Abstract The InSight seismometers have recorded more than 1,300 events. Ninety-eight of these, named the low-frequency (LF) family, show energy predominantly below 1 Hz down to ~0.1 Hz. The Marsquake Service identified seismic phases and computed distances for 42 of these marsquakes, 24 of which have backazimuths. Hence, the locations of the majority of LF family events remain undetermined. Here, we use an envelope shape similarity approach to determine event classes and distances, and introduce an alternative method to estimate the backazimuth. In our analysis, we use the highest quality marsquakes with known distances as templates, including the largest event S1222a, and assign new distances to similar group of events for which distance estimates were not previously available. We find the Tharsis region to be more active than initially perceived on the basis of 5 newly located events near Valles Marineris and Olympus Mons. We relocate two marsquakes with little or no S-wave energy in the NE of the Elysium Bulge. The event epicenters in Cerberus Fossae follow a north-south trend due to uncertainties in location, while the fault system is in the NW-SE direction; therefore, these events are re-projected along the observed fault system based on our interpretations. The marsquakes in our interpreted catalog are predominantly observed in the northern hemisphere of Mars above the equatorial dichotomy boundary.

Plain Language Summary InSight's seismometer recorded more than 1,300 events since landing on the surface of Mars in November 2018 until it retired in December 2022. Most of the events InSight recorded are at high frequencies ≥2.4 Hz. The rest of the events, named the low-frequency family, produce signals that travel through the planet's interior, allowing us to understand the interior structure when event locations can be determined. In order to use the single-station approaches for computing the distance and the angle between the station and an event, at least two clear seismic phase arrivals (such as P- and S-waves for distance and P-wave for event angle) are required. However, marsquakes are often weak and do not always exhibit clear seismic phases; therefore, they cannot be assigned distances using traditional techniques. Here, we use the well-understood, highest-quality events as templates to investigate and assign a source region to the weaker seismic signals. Seismicity on Mars occurs mostly along or north of the boundary between the southern highlands and northern lowlands. Valles Marineris is seismically more active than previous catalogs of located events imply. Further, we show evidence that two events likely originate from the Olympus Mons region.

Key Points:

- We use a similarity analysis and high quality marsquake templates from InSight to estimate distances of additional events
- Combining this with new backazimuth estimates we can relocate marsquakes and update the seismicity map of Mars
- Our results suggest clusters of seismicity have occurred nearby Valles Marineris and Olympus Mons

Supporting Information:

Supporting Information may be found in the online version of this article.

Correspondence to:

S. Ceylan,
savas.ceylan@erdw.ethz.ch

Citation:

Ceylan, S., Giardini, D., Clinton, J. F., Kim, D., Khan, A., Stähler, S. C., et al. (2023). Mapping the seismicity of Mars with InSight. *Journal of Geophysical Research: Planets*, *128*, e2023JE007826. https://doi.org/10.1029/2023JE007826

Received 13 MAR 2023
Accepted 31 JUL 2023

Author Contributions:

Conceptualization: S. Ceylan, D. Giardini, J. F. Clinton
Data curation: S. Ceylan, J. F. Clinton, D. Kim, G. Zenhäusern
Formal analysis: S. Ceylan, D. Giardini, J. F. Clinton, D. Kim, A. Khan, S. C. Stähler
Funding acquisition: D. Giardini, P. Lognonné, W. B. Banerdt
Investigation: J. F. Clinton, D. Kim, A. Khan
Methodology: S. Ceylan, D. Giardini, D. Kim, S. C. Stähler

© 2023. The Authors.
This is an open access article under the terms of the Creative Commons Attribution License, which permits use, distribution and reproduction in any medium, provided the original work is properly cited.

1. Introduction

The Mars InSight mission (Banerdt et al., 2020) retired on 21 December 2022, after approximately 4 years (1,446 sols or Martian days) of successful operation. The mission deployed the first seismic station (SEIS) on the surface of the planet, comprising both a very broadband (VBB) and a short-period seismometer (Lognonné et al., 2019, 2020). The InSight payload also contained wind and pressure sensors for observing the Martian atmosphere (Banfield et al., 2020), which provided crucial information for discriminating seismic events from environmental noise sources; the HP^3 temperature probe (Spohn et al., 2022); and the robotic arm and cameras used for deploying SEIS and HP^3 on the ground(Banerdt et al., 2020).

Throughout the mission, the Marsquake Service (MQS; Clinton et al., 2018) cataloged 1,323 signals of seismic origin (Table S1 in Supporting Information S1; InSight Marsquake Service, 2023) in the data set (Ceylan et al., 2022; Clinton et al., 2021). Ninety-eight of these events are part of the low-frequency (LF) event family showing energy predominantly below 1 Hz. The rest of the events contain energy mostly above 2.4 Hz and are classified as the high-frequency (HF) family. MQS released the seismicity catalog in every 3 months with a

Project Administration: P. Lognonné, W. B. Banerdt
Software: S. Ceylan
Supervision: D. Giardini, J. F. Clinton
Validation: S. Ceylan, D. Kim, A. Khan, S. C. Stähler, P. Lognonné, W. B. Banerdt
Visualization: S. Ceylan
Writing – original draft: S. Ceylan, D. Giardini, J. F. Clinton, D. Kim, A. Khan, S. C. Stähler, G. Zenhäusern, P. Lognonné, W. B. Banerdt
Writing – review & editing: S. Ceylan, D. Giardini, J. F. Clinton, D. Kim, S. C. Stähler

3-month delay (Clinton et al., 2021). Each catalog version comprises the complete collection of events from the previous release, as well as any new events observed during the subsequent 3-month cycle. The version 14 (V14) is the final release following InSight's retirement (InSight Marsquake Service, 2023). We refer the reader to Clinton et al. (2021) for a detailed overview of the seismicity, event types, and catalog content.

For events in the LF family, when seismic body wave phases can be identified (typically direct P and S, or their surface reflections PP and SS for distant events $\gtrsim$100°), MQS determines the event's geographical location by estimating distance and angle with respect to north as seen from InSight (backazimuth) separately. The distance estimate uses relative P and S travel times against theoretical travel times from the model set of Stähler et al. (2021) following the single station location algorithms described in Khan et al. (2016) and Böse et al. (2017). The full location of an event is obtained when a backazimuth can also be reliably determined (Böse et al., 2017). In the current MQS practice (since the V12 catalog (InSight Marsquake Service, 2022)), this follows the method described in Zenhäusern et al. (2022), using the polarization attributes of both P- and S-waves estimated in the time-frequency domain (Schimmel & Gallart, 2004).

In the V14 catalog, MQS computed distances for 42 of the 98 LF family events (Figure 1a). Twenty-four of these events are fully located with a backazimuth, while the remaining events only have a distance estimate and are quality B or C (Table S1 in Supporting Information S1), and two events have backazimuths without a distance. The vast majority of the fully located events cluster at distances between 25° and 35° with a backazimuth pointing toward the east, the Cerberus Fossae (CF) region (Figure 1a).

The most distant marsquake (S0976a; Figure 1) was observed on 25 August 2021, at a distance of 146 ± 7° from InSight and a backazimuth of 101 ± 25°, locating the event in the Valles Marineris (VM) region (Horleston et al., 2022). The event is in the core-shadow, which allowed the observation of core-crossing SKS body waves (Irving et al., 2023). Two events (S1000a and S1094b) showed the first clear indication of seismic surface wave arrivals (Kim et al., 2022). Both of these events were later confirmed as distant impacts (Posiolova et al., 2022; hereinafter, referred to as S1000a^I and S1094b^I to indicate the events are impacts for brevity) with Mars-calibrated moment magnitudes (Böse et al., 2018, 2021) of M_W^{Ma}4.0 ± 0.2 and 4.1 ± 0.2 (Figure S1 in Supporting Information S1) and crater diameters of 130 and 150 m, respectively. Furthermore, 6 HF family events within 300 km of InSight have also been confirmed as impacts (Daubar et al., 2023; Garcia et al., 2022), which show dispersive acoustic signals propagating along a waveguide in their coda, with strong linear polarization pointing toward the source. Finally, the largest marsquake (M_W^{Ma}4.6 ± 0.3) recorded by InSight is S1222a (Kawamura et al., 2023), which occurred on 4 May 2022 (Figure S1 in Supporting Information S1).

Marsquakes are low-amplitude and the background seismic noise at InSight's location is highly variable; therefore, the large number of noisy events is not surprising. Interpreting these noisier events is challenging and phase arrivals cannot be assigned to determine distances in the standard manner. In order to overcome this limitation, Giardini et al. (2020) introduced a qualitative alignment-based methodology, where weak marsquakes are assigned a distance depending on their envelope similarities with the highest-quality events, whose distances were assumed fixed or anchored. In their approach, the events are visually aligned based on the predicted travel times of seismic phases using a reference interior model. Since V3 catalog (InSight Marsquake Service, 2020), MQS included distance estimates from this visual alignment approach, using a recent reference model from Stähler et al. (2021), although phase-based distance estimates were preferred when available.

Given the retirement of InSight and the availability of a fully archived seismic data set, we take the opportunity to extend the previous analysis of the LF events by the visual alignment approach. Here, we apply the Dynamic Time Warping (DTW) algorithm (Sakoe & Chiba, 1978) to the LF envelopes and quantify the similarities observed across the LF events by using those with the highest SNR (signal to noise ratio) as reference events. Our alignment of event envelopes enables the relocation of relatively weaker LF events and provides an update to the original seismicity map of Giardini et al. (2020). We interpret the new seismicity on Mars in light of the known or expected tectonically active regions. Our findings highlight the potential value of utilizing previously under-explored MQS events with low SNR, and will have implications for future studies on the interior structure of Mars.

2. Data and Methods

For our analysis, we use spectral envelopes derived from the 20 samples-per-second (sps) VBB waveform data for the LF family events cataloged during the entire mission. All the events and waveforms (InSight Mars SEIS

21699100, 2023, 8, Downloaded from https://agupubs.onlinelibrary.wiley.com/doi/10.1029/2023JE007826 by Cochrane France, Wiley Online Library on [07/09/2023]. See the Terms and Conditions (https://onlinelibrary.wiley.com/terms-and-conditions) on Wiley Online Library for rules of use; OA articles are governed by the applicable Creative Commons License

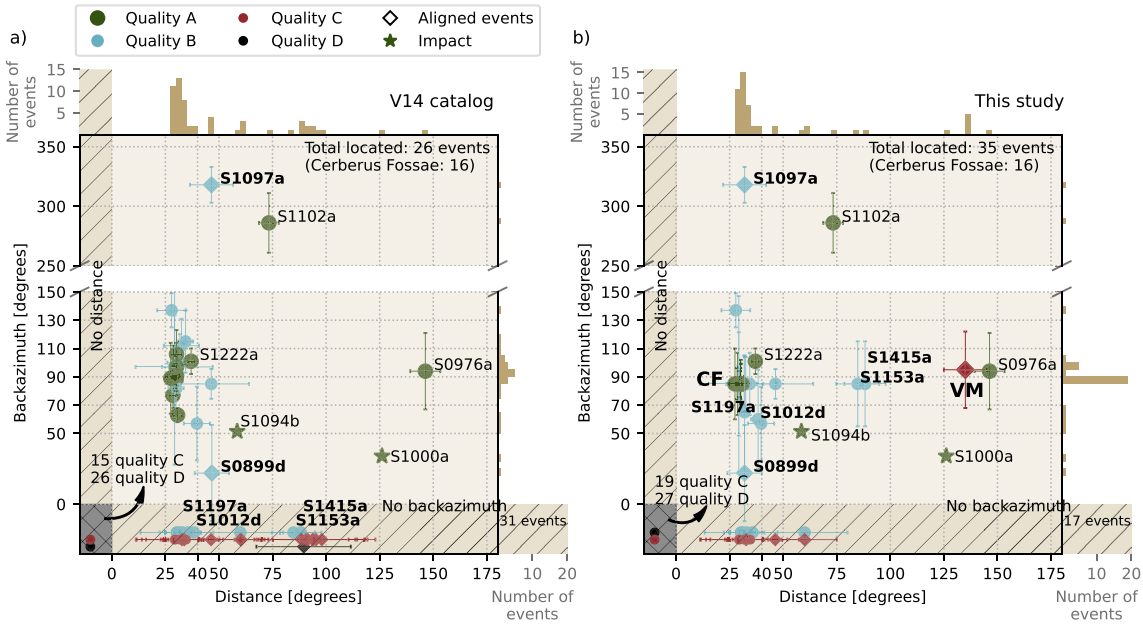

Figure 1. Distance and backazimuth distribution of the LF-family events in (a) the V14 catalog (InSight Marsquake Service, 2023), and (b) this study. The confirmed impacts, S1000a^{I} and S1094b^{I}, are denoted by stars. The 6 events labeled in bold-face have locations that are newly introduced or are modified in this study. Note a number of events without backazimuths also have their distances revised. Diamonds indicate events in V14 where the distance is only provided by visual alignments. The colors and marker sizes show the event qualities as indicated in Table S1 of Supporting Information S1. The histograms indicate the number of events for distance (top) and backazimuth (right). A majority of the catalog includes events at distances around 30° and a backazimuth toward east (80–100°), pointing to the Cerberus Fossae region. The hatched regions show events without backazimuth or distance estimates. The errors bars show the uncertainties in distance and backazimuth. See Figure S1 in Supporting Information S1 for the distance and M_W^{Ma} distributions, and Table S2 in Supporting Information S1 for a summary of re-evaluated events and our modifications. CF, Cerberus Fossae; VM, Valles Marineris.

Data Service, 2019a, 2019b) are publicly available with the release of the V14 catalog (InSight Marsquake Service, 2023). A breakdown of the catalog, including the HF events, is provided in Table S1 of Supporting Information S1.

Our method builds on the visual alignment approach of Giardini et al. (2020). In the visual alignments, the envelopes of both low SNR and high-quality events are compared, and weaker events are assigned a relative distance using the envelope shape similarities, theoretical travel time curves and the events with pick-based distances as anchors. However, the low SNR events are often found to be similar to multiple template events, that is, in the shape and length of their S-wave coda. Consequently, interpretation of events is often challenging and ambiguous.

In order to address these particular cases, we employ the Dynamic Time Warping (DTW; Sakoe & Chiba, 1978) algorithm to measure event similarity using the shape of their spectral envelopes (Figures 2 and 3). Additionally, we use an alternative approach to determine new backazimuths for a subset of events using grid search for the same envelopes when MQS does not report any value, as illustrated in Figure 4. Finally, we provide distances for the events with lower SNR by finding the best matches to the collection of high-quality template events, with addition insights from backazimuths in some cases, and separate the seismicity into classes (Figure 5). In our analysis, we focus on signal similarity as a main criterion across different seismic events and leave out other complexities associated with their source (Stähler et al., 2021) or 3D structural effects (Kim, Duran, et al., 2023; Plesa et al., 2022), which still remain largely unaccounted for.

2.1. Similarity Analysis

The data processing workflow we use to generate the envelopes is summarized in Figure S2 of Supporting Information S1. First, we remove the instrument response to obtain acceleration time series and rotate the VBB data into the ZNE (vertical-north-east) coordinate frame. Then, we compute spectrograms for all three components in linear amplitude scale, using a window length of 30 s and an overlap of 60%. Finally, we obtain the envelopes by summing the spectral amplitudes along the frequency axis between 0.25 and 0.9 Hz. This frequency range is rich

21699100, 2023, 8, Downloaded from https://agupubs.onlinelibrary.wiley.com/doi/10.1029/2023JE007826 by Cochrane France, Wiley Online Library on [07/09/2023]. See the Terms and Conditions (https://onlinelibrary.wiley.com/terms-and-conditions) on Wiley Online Library for rules of use; OA articles are governed by the applicable Creative Commons License

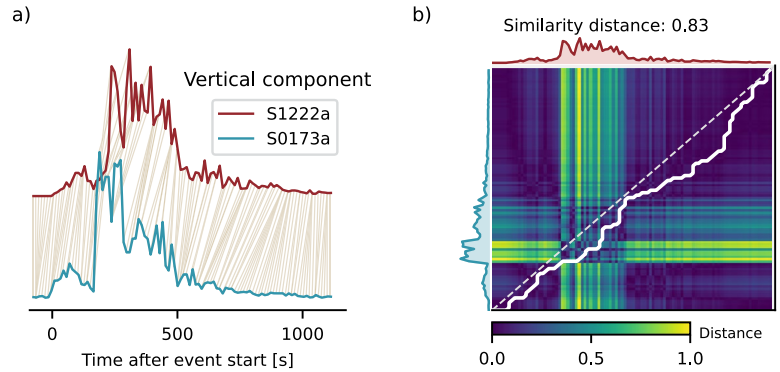

Figure 2. Example of the DTW method (Sakoe & Chiba, 1978) to determine the shape similarity between the spectral envelopes of two of the high-quality marsquakes, S1222a and S0173a. (a) The final optimal point-wise pairings between the event envelopes. The light-brown lines indicate matching data points with minimum distance in $\|L_1\|$ norm. (b) The warping path and cross-similarity matrix. The color bar shows the normalized distance measure for similarity, with larger values indicating less similarity. The warping path would be perfectly diagonal (dashed line) if the envelopes were identical. The deviation from the ideal path for these two events is reasonably close to the diagonal.

in energy for the majority of LF family events (Ceylan et al., 2022). The upper frequency bound is intentionally below 1 Hz to avoid an artifact caused by the onboard electronics (Zweifel et al., 2021). The envelopes have a sample point every 12 s. Although different frequency ranges, window lengths and overlaps can be used, the selected parameters are preferred through experience gathered throughout the mission so as to allow for comparison of events from different distances. We use the vertical component for measuring envelope shape similarities since it is the least-contaminated by atmospheric disturbances.

For data regularization in advance of the DTW (Figures 2 and 3), a short time-window around significant glitches in the time series are masked in the spectral envelopes. Glitches are ubiquitous artifacts observed in the data (Ceylan et al., 2021; Scholz et al., 2020), most likely caused by thermal expansion of the spacecraft, the cable connecting spacecraft and SEIS, or the SEIS components itself (Scholz et al., 2020). They generally show a signal shape similar to the impulse response of the seismometer and can exceed the amplitude of seismic phases by several orders of magnitude. Since their amplitude can vary significantly, automatic detection is not trivial and unrecognized glitches may lead to inaccurate interpretations (Kim et al., 2021). Therefore, MQS resorts to identify the glitch windows manually. We mask the glitches (as reported by MQS) by replacing the original envelope values with the mean of adjacent data points. The spectral envelopes start 90 s prior to the energy onset as marked in the V14 catalog. The end times are manually assigned for the few events that have a very long duration (>1 hr); otherwise, we use the signal end from the catalog (InSight Marsquake Service, 2023) assigned by MQS operators with the aid of spectrograms. For shape similarity metrics, the point-wise distances in Figure 2a are computed using the $\|L_1\|$ norm because of its stability and relative insensitivity to noisy time series. The final similarity values (Figure S3 in Supporting Information S1) are normalized with the warping path length to account for differences in the duration of the time series.

We utilize the DTW method as a tool for quantification to determine the most probable template event when an event shares shape similarities with multiple high-quality marsquakes. The DTW method is not suitable to use in a fully automated style for our purposes. For instance, an event with no apparent S-wave energy may show a relatively higher degree of similarity to another event with strong S-wave (e.g., S1097a and S0235b in Figures 3a and 3b). Therefore, an a-priori knowledge of events for their available phase picks, polarization attributes and P- and S-wave coda lengths are required for interpretation.

2.2. Backazimuth Estimation

Backazimuth is defined as the angle between the seismic station and epicenter with respect to north in a station-centric coordinate frame. MQS initially determined backazimuth from the three-component particle motions in the time domain (Böse et al., 2017), and subsequently migrated to a more rigorous approach using polarization measured from both P and S-waves in the frequency-time domain (Zenhäusern et al., 2022). MQS does not assign backazimuths when the results from either method are interpreted to be unstable.

21699100, 2023, 8, Downloaded from https://agupubs.onlinelibrary.wiley.com/doi/10.1029/2023JE007826 by Cochrane France, Wiley Online Library on [07/09/2023]. See the Terms and Conditions (https://onlinelibrary.wiley.com/terms-and-conditions) on Wiley Online Library for rules of use; OA articles are governed by the applicable Creative Commons License

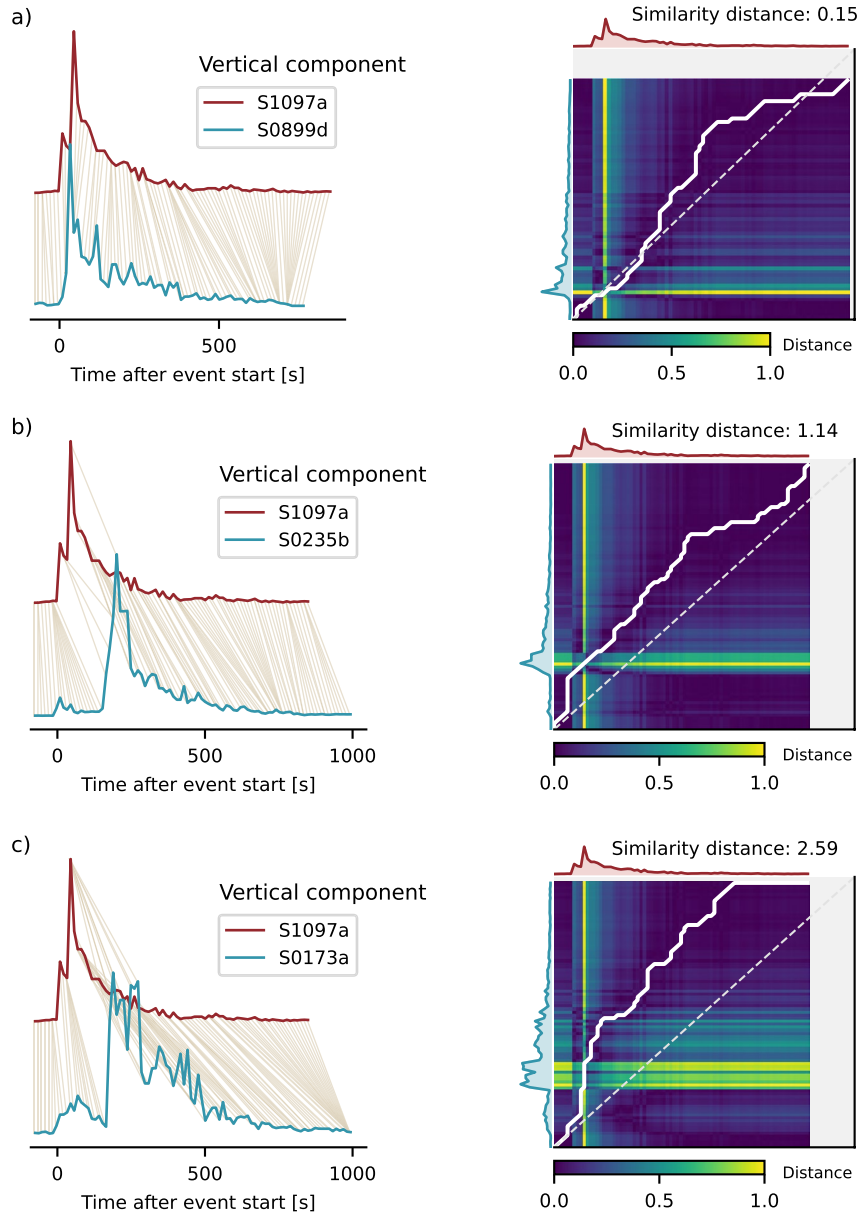

Figure 3. Similarity analysis for S1097a, a low-frequency (LF) QB event without an assigned distance in the V14 catalog, against three template events. The final similarity distances in $\|L_1\|$ norm are indicated in the warping path panels, where smaller values indicate higher level of similarity (Figure S3 in Supporting Information S1). The event is most similar to S0899d (a), another LF QB event without a pick-based distance in the catalog. Therefore, S1097a clusters within the same class. Note that the envelope shape is also significantly similar to S-wave coda of S0235b (b). The degree of similarity decreases for other templates such as S0173a as shown in (c).

The MQS method relies on seismic phases with a high degree of polarization (DOP). However, for strongly scattered waveforms, such as the so-called HF events, this method has generally not found to work. It was shown that instead, the energy ratio on the horizontal components can give an indication of backazimuth for such events, albeit with an ambiguity of 180° (Stähler et al., 2022). In an attempt to increase the number of events with assigned backazimuths, we test this approach on LF marsquakes. In order to find the most plausible rotation angle range, we rotate the horizontal components for 360° with an increment of 2° and compute envelopes. Ideally, in the presence of P-waves, the energy ratio of vertical (Z) and radial (R) components compared to the transverse (T) must be maximized when the rotation is in the same direction as the true backazimuth. As a reliability check, the transverse-to-radial ratio should have maxima at 90° perpendicular to the vertical-to-transverse component ratio.

21699100, 2023, 8, Downloaded from https://agupubs.onlinelibrary.wiley.com/doi/10.1029/2023JE007826 by Cochrane France, Wiley Online Library on [07/09/2023]. See the Terms and Conditions (https://onlinelibrary.wiley.com/terms-and-conditions) on Wiley Online Library for rules of use; OA articles are governed by the applicable Creative Commons License

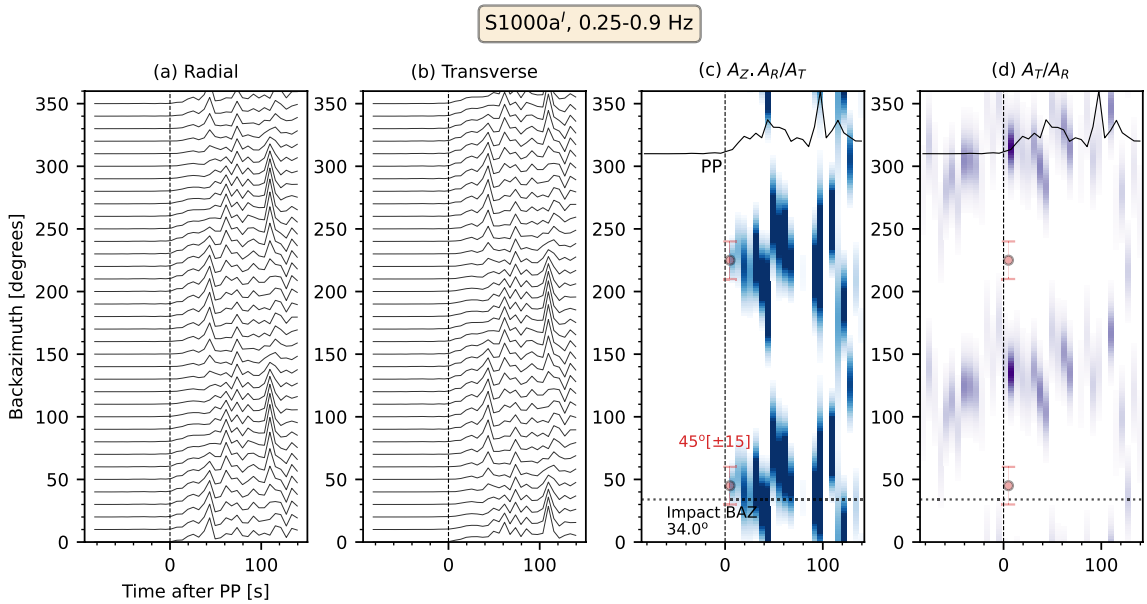

Figure 4. Validation of envelope-based grid search approach for backazimuth estimation using S1000a^I. The impact crater is detected 126.09° away from InSight and at a backazimuth of 34° (Posiolova et al., 2022). The vertical dashed lines at zero time on each panel indicate the PP phase arrival time. (a) and (b) show the rotated horizontal envelopes, computed for frequencies between 0.25 and 0.9 Hz. The envelope amplitudes are normalized using the maximum of the vertical component for visualization purposes. (c) and (d) denote combined vertical (Z) and radial (R) to transverse (T) and T/R ratio, respectively. The orange circles and error bars show the preferred backazimuth pick with the ambiguity, computed using envelope amplitudes prior to normalization. For reference, the Z-component envelopes are plotted at the top of (c) and (d). The horizontal dotted lines in (c) and (d) show the true backazimuth. The color scale in (c) is saturated to make the amplitudes after the PP more visible.

Using the two distant impacts as well as two of the high quality events S0235b (SNR 992) and S1222a (SNR 3.7×10^6), we demonstrate that our approach can recover similar backazimuths to the other methods (Figure 4 and Figures S4–S6). In our test cases, the element-wise product of *Z* and *R* components (*Z.R/T*) better accentuates the results (Figure 4c and Figures S4–S6 in Supporting Information S1), which makes picking backazimuths easier. We choose the backazimuth values using the first concentrated amplitude ratios in the time window directly after the initial phase arrivals and assign the uncertainties visually (Figure 4).

3. Results and Discussion

The InSight seismicity catalog (Ceylan et al., 2022; Clinton et al., 2021) is a collective inventory of work from the InSight science team that includes not only the locations provided by MQS, but also locations of known impacts (Garcia et al., 2022; Posiolova et al., 2022), alternative source interpretations (Kedar et al., 2021), seismic phase picks (Drilleau et al., 2022; Durán, Khan, Ceylan, Zenhäusern, et al., 2022; Khan et al., 2021; Stähler et al., 2021), and distance and seismic phase assignments from the visual alignments (Giardini et al., 2020). Our analysis below provides new, updated alignments that allow us to assign distances to substantially more LF events, classify events into classes or groups, and enable us to re-evaluate our understanding of Martian seismicity. A summary of the work is shown in Figure 5, where the various event groups are present in terms of their distance from the InSight lander. These results can be expected to be included in final, post-mission catalog releases from MQS.

The seismicity map of Mars as contained in the MQS V14 catalog (InSight Marsquake Service, 2023) is summarized in Figure 6a, while our interpretation resulting from this analysis is in Figure 6b (also see Figures S10–S12 for each class discussed below). The seismicity on Mars appears to occur along or to the north of the dichotomy boundary, which is the sharp elevation contrast between the lowlands in the northern hemisphere and highlands in the south. Furthermore, it is notable that two of the three template events from distances >90° are the S1000a^I and S1094b^I impacts.

3.1. Distant Events Cluster

The so-called distant events (Figure 7) are a class of seismic signals that are bound between the two most distant template events, S1000a^I and S0976a. The low SNR signals that match this group lack any indication of P-energy

21699100, 2023, 8, Downloaded from https://agupubs.onlinelibrary.wiley.com/doi/10.1029/2023JE007826 by Cochrane France, Wiley Online Library on [07/09/2023]. See the Terms and Conditions (https://onlinelibrary.wiley.com/terms-and-conditions) on Wiley Online Library for rules of use; OA articles are governed by the applicable Creative Commons License

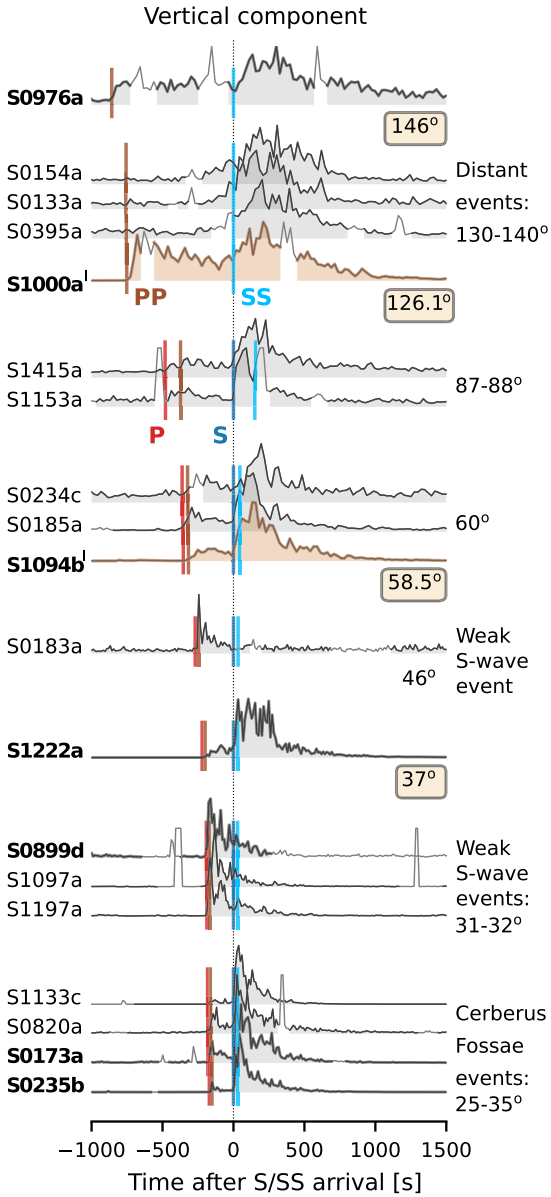

Figure 5. Overview of event classes. Each class is indicated by the label on the right. Template events are indicated by bold lines and font. Time series show the envelopes computed from the vertical component acceleration data for frequencies 0.25–0.9 Hz. The light-gray parts of the envelopes show the data with glitches; note the glitches are masked for similarity processing. The two envelopes in tan color are the known impacts. The distances from V14 are indicated on the right side for all template events outside of the Cerberus Fossae cluster. The zero time is the first arriving theoretical S-wave (S or SS depending on the distance) from a reference model (Ceylan et al., 2022; Stähler et al., 2021). Theoretical arrival times for P, S, PP, and SS phases are marked and labeled. S0899d, S1097a, and S1197a belong to the same class with S0183a, but lie closer to InSight at around 32°. The envelope amplitudes are in log-scale to emphasize small-scale similarities. The envelopes for events >50° are processed with a window length of 60 and 30 s for the rest, all with a 50% overlap.

and exhibit relatively long energy packages, which we interpret as S-wave and its coda. The visual alignments placed these events at distances >90° using the length of the S-wave coda as a proxy for distance (Figure 6a and Figure S11 in Supporting Information S1). The two distant template events, the only ones known to lie beyond the core shadow based on clear phase picks, did not occur until late in the mission over 2.5 years after landing. Therefore, although the weak events now assigned at this distance occurred early on the mission, there was no possibility to constrain their event distances until recently.

MQS locates S0976a in the VM region (Horleston et al., 2022), 146 ± 7° away from InSight. S1000a^{I} occurred in Tempe Terra at a distance of 126° (Figure 6a) (Posiolova et al., 2022). In this context, we note that an independent joint seismic event-location and structure-inversion scheme predicts a location for S1000a^{I} in excellent agreement with the imaged location (Durán, Khan, Ceylan, Charalambous, et al., 2022). The S-wave coda lengths for distant events are more comparable to S1000a^{I} as it is shorter than S0976a (Figures 5 and 7), suggesting that these events occurred at a distance range of ∼130–140°, possibly closer to S1000a^{I}.

Considering the lack of any energy that we interpret to be P-wave, as well as the emergent nature of the S-energy, the envelope-based backazimuth approach was not useful to further constrain locations for these events. The only evidence of tectonic-related seismic activity (S0976a) at these distances is from VM.

VM is amongst the largest canyons in the solar system (Coles et al., 2019). Together with the Tharsis province, it has been proposed as one of the most seismically active regions on Mars, supported by both surface faulting observations (Golombek et al., 1992) and joint inversion of gravity and topography data (Gudkova et al., 2017). Furthermore, in an analysis of boulder falls in VM, Senthil Kumar et al. (2019) suggest that the region must have been seismically active in its recent past. Moreover, the global stress distributions indicate that together with the Olympus Mons, VM is one of the most prominent features with a high sub-crustal stress accumulation caused by a crustal loading of Tharsis province (Tenzer et al., 2015). Thus, it is reasonable to assume that the region is more active than might be suggested on account of the observation of a single event from InSight. Here, we assign these events at a distance of 130–140°, and suggest that one of the potential source regions could be in the western part of VM (Figures 6b and 6d). However, we cannot entirely rule out other possible locations within the Tharsis province.

3.2. Assigning Locations to S1153a and S1415a

In V14 catalog, MQS provides only distance estimates for S1153a and S1415a at 84.8 ± 10° and 88.2 ± 9.6°, respectively. In addition to being the only events in the catalog with phase-based distances at this distance, the frequency content of the events is also remarkably similar (Figure S8 in Supporting Information S1). Furthermore, they show a high degree of envelope shape similarity in all three components (Figure 8a and Figure S7d in Supporting Information S1), suggesting that most likely both events originated from the same region.

21699100, 2023, 8, Downloaded from https://agupubs.onlinelibrary.wiley.com/doi/10.1029/2023JE007826 by Cochrane France, Wiley Online Library on [07/09/2023]. See the Terms and Conditions (https://onlinelibrary.wiley.com/terms-and-conditions) on Wiley Online Library for rules of use; OA articles are governed by the applicable Creative Commons License

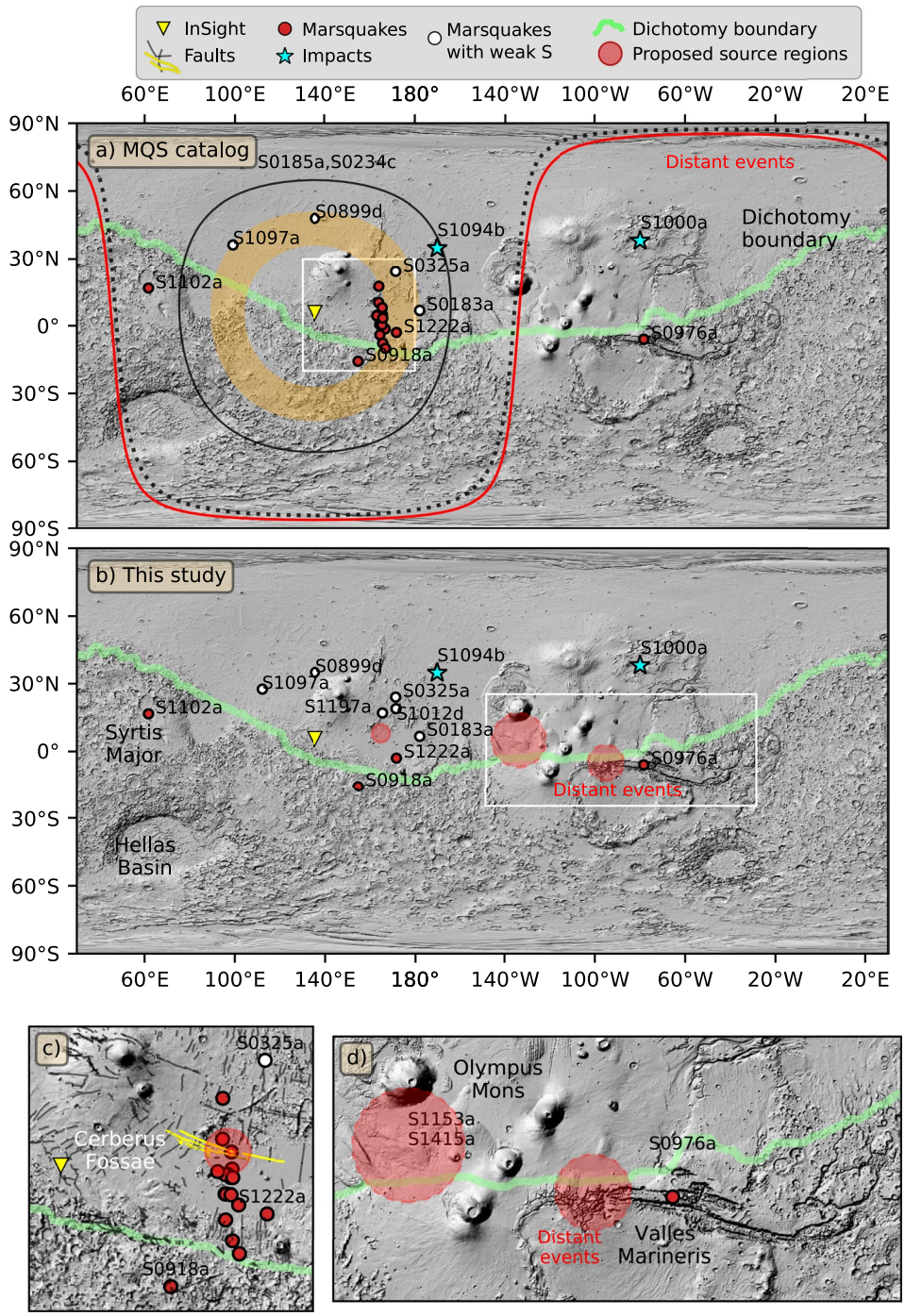

Figure 6. Proposed regions of seismic activity. (a) The current state from the V14 catalog (InSight Marsquake Service, 2023), including the interpretations from the visual alignments adopted since Giardini et al. (2020). The orange-colored ring around InSight denotes the distance range of 32–46° for the events with weak or no S-wave. The red curve at 90° represents the distant events class. The dotted curve indicates the distances for S1153a (84.8 ± 10°) and S1415a (88.2 ± 9.6°) as reported by MQS. (b) Our interpretation of the seismicity. The light red shaded circles indicate regions where there are clusters of multiple events. Symbols sizes indicate the extent of the region, not location uncertainties. Zoomed views around the Cerberus Fossae and Valles Marineris are in (c) and (d), also marked with white rectangles in (a) and (b), respectively. Fault locations in (c) around Cerberus Fossae do not reflect large uncertainties in backazimuth, allowing us to interpret that all events are associated with the fault system. The fault lines in (c) are from Knapmeyer et al. (2006) and Perrin et al. (2022), where the faults in yellow show the Cerberus Fossae system. The background map and the equatorial dichotomy boundary are from Smith et al. (2001) and Andrews-Hanna et al. (2008), respectively.

21699100, 2023, 8, Downloaded from https://agupubs.onlinelibrary.wiley.com/doi/10.1029/2023JE007826 by Cochrane France, Wiley Online Library on [07/09/2023]. See the Terms and Conditions (https://onlinelibrary.wiley.com/terms-and-conditions) on Wiley Online Library for rules of use; OA articles are governed by the applicable Creative Commons License

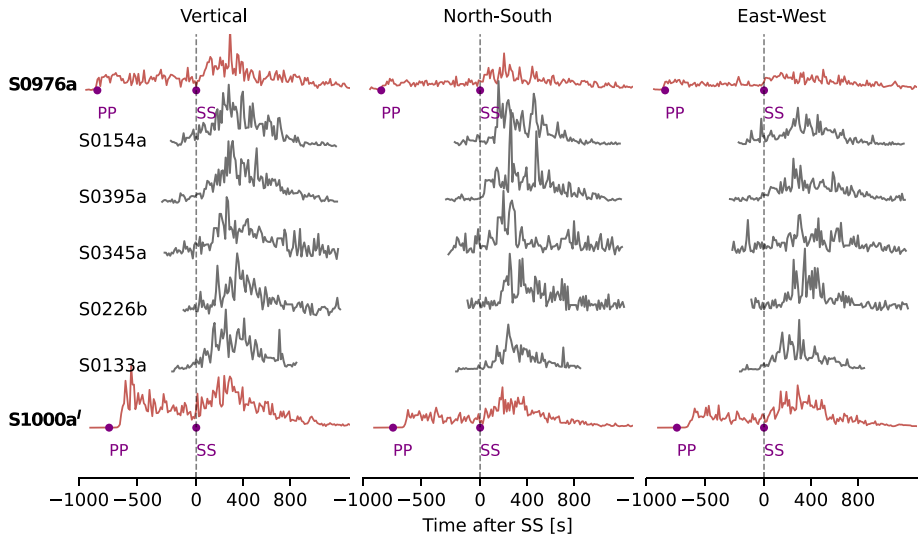

Figure 7. The class of most distant events, bound by the template events S0976a and S1000a′ shown in red and with bold-face font. The purple dots are the Marsquake Service phase picks used to determine distances for the templates. Time series show normalized vertical component envelopes. The template events are aligned on their SS phase picks. Other events are aligned with their energy onset which we interpret as S-waves taking the vertical component as reference.

MQS does not assign a backazimuth to either of these events due to their emergent P-arrivals and contaminated waveform characteristics (Figure S8 in Supporting Information S1). Applying the envelope-based grid search approach for S1153a, we obtain a backazimuth estimate of 85 ± 30° with a 180° ambiguity (Figure 8a), which places the event either at the boundary of Terra Sabaea and Western Syrtis Major or in a region SW of Olympus Mons. A reliable backazimuth pick was not possible for S1415a, although the P-wave energy partitioning between the horizontal components imply a value similar to S1153a in a more NE-SW direction (Figure 8b). Considering the large uncertainties for S1153a, we assume both events occurred roughly in the same region. Given the presence of faulting in late Amazonian terrain south-east of Olympus Mons (Hargitai & Gulick, 2018), a source in this general region seems more plausible and we locate these two events around Olympus Mons (Figure 6b and Figure S10 in Supporting Information S1).

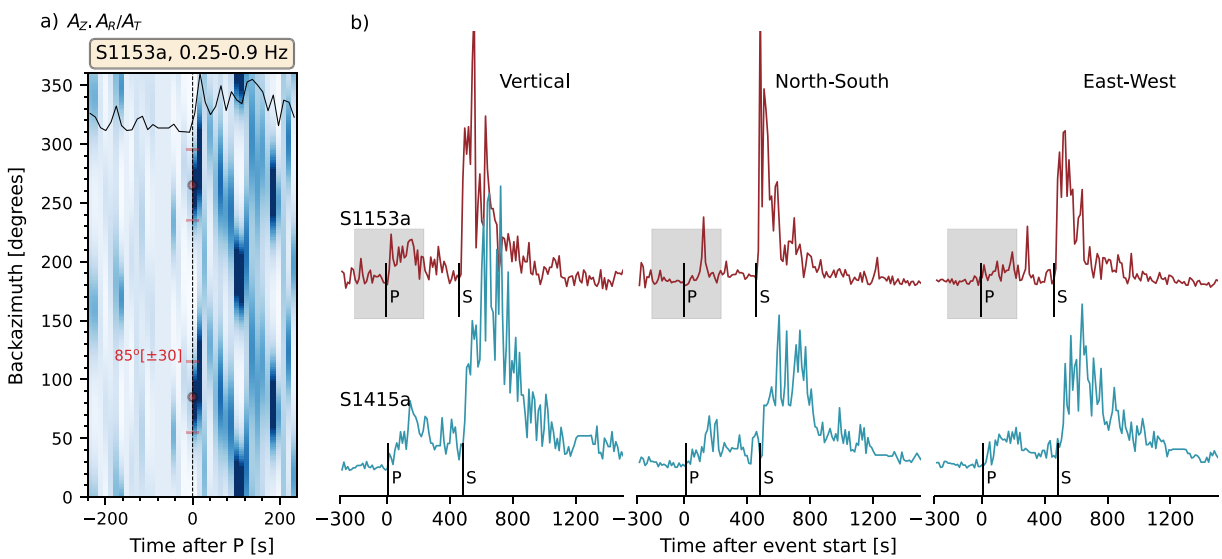

Figure 8. Backazimuth analysis and envelopes for the S1153a and S1415a event pair. (a) Backazimuth estimation for S1153a. (b) Three-component envelopes computed between 0.25 and 0.9 Hz using the very broadband data in acceleration. The shaded region on the S1153a envelopes denote the time window shown in (a). Seismic phase picks from Marsquake Service are shown as black dots. The picking uncertainties for P and S are ±20 and ±10 s, respectively for both events. See Figure S7d in Supporting Information S1 for the similarity warping path.

21699100, 2023, 8, Downloaded from https://agupubs.onlinelibrary.wiley.com/doi/10.1029/2023JE007826 by Cochrane France, Wiley Online Library on [07/09/2023]. See the Terms and Conditions (https://onlinelibrary.wiley.com/terms-and-conditions) on Wiley Online Library for rules of use; OA articles are governed by the applicable Creative Commons License

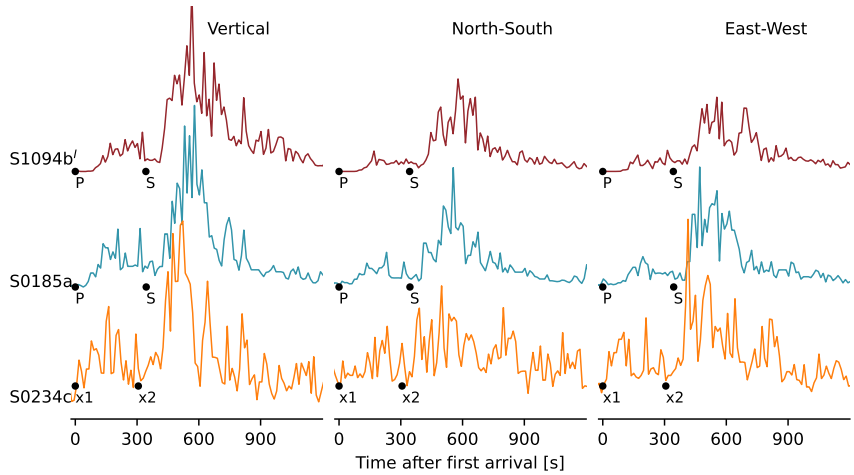

Figure 9. S1094b^{I} class. The dots are the phase picks from the V14 catalog. Marsquake Service identified two phases for S0234c and labeled them as unknown (x1 and x2).

It is noted that in the V14 catalog and seen in Figure 1a, there is a cluster of aligned events assigned also to this distance. As described in the previous subsection, all these aligned events have been moved further away from InSight to VM.

3.3. Events Near to S1094b^{I}: S0185a and S0234c

The S1094b^{I} impact crater was detected in Amazonis Planitia at a distance of 58.5° with a backazimuth of 51.4° (Posiolova et al., 2022). Two relatively weak events S0185a and S0234c are shown to have large similarity, as demonstrated in Figure 9 and Figure S7b in Supporting Information S1. No surface waves have been identified from these events unlike the S1094b^{I} record (Kim et al., 2022). The distance for S0185a is calculated by MQS as 60 ± 20° or 63.1 ± 4.3° by Durán, Khan, Ceylan, Zenhäusern, et al. (2022). S0234c is assigned a distance of around 70° through visual alignment. Neither of the events have MQS assigned backazimuths. Our similarity metrics confirm that S1094b^{I} is very similar to S0185a, and similar to S0234c (Figure S7 in Supporting Information S1). Therefore, we do not modify the previously reported distances.

No reliable backazimuth for either S0185a or S0234c can be obtained from our envelope-based grid search approach. The next marsquake with a full seismically estimated location is S1102a (distance 73.3 ± 5°), located in Syrtis Major Planum (Figure 6). The MQS distances for S0185a and S0234c coincide well with the eastern portion of Syrtis Major Planum. However, S0185a envelopes are less similar to S1102a than S1094b (Figure S7c in Supporting Information S1), and it is difficult to propose a specific source region without any indication of backazimuth for either of the events.

Table 1
Location Parameters of the S0899d Class

Event name	V14 Distance (°)	V14 BAZ (°)	This study Distance (°)	This study BAZ (°)
S0183a	46.0 ± 17.0	85 ± 17	–	–
S0899d	46.7 ± 10*	22 ± 30	32 ± 10	–
S1197a	32.0 ± 1.5	–	–	65 ± 40
S1097a	46.2 ± 10*	318 ± 20	32 ± 10	–
S1012d	38.2 ± 3.3	–	–	60 ± 35
S0325a	39.7 ± 6.1	57 ± 20	–	–

Note. The V14 distances with asterisks are assigned using the visual alignment rather than phase picks. We modified the previously assigned distances for S0899d and S1097a using new S-picks as shown in Figure 7, and calculated new backazimuths for S1197a and S1012d (Figure 11). BAZ, backazimuth.

3.4. Events Similar to S0899d: Marsquakes With Weak or No S-Waves

S0899d exhibits a strong arrival that can clearly be attributed to a P-wave based on its vertical polarization, which indicates that the event comes from a direction to the north of InSight with a backazimuth of 22 ± 30° (Table 1, Figure 6). A subset of weak marsquakes, like S0899d, also show little-to-no S-wave energy (Figure 10) in the vertical component or have an S–to–P ratio ~1. The template for this class of events is S0899d, which does not have a pick-based location, although visual alignments suggest a distance of ~46° due to its similarity to S0183a.

Here, using the envelopes, we identify for the first time S-wave arrivals for S0899d and S1097a on the horizontal components (Figure 10), and modify their aligned distances from 46° to 32° by aligning the event against the theoretical travel times from the reference model (Figures 5 and 6).

21699100, 2023, 8, Downloaded from https://agupubs.onlinelibrary.wiley.com/doi/10.1029/2023JE007826 by Cochrane France, Wiley Online Library on [07/09/2023]. See the Terms and Conditions (https://onlinelibrary.wiley.com/terms-and-conditions) on Wiley Online Library for rules of use; OA articles are governed by the applicable Creative Commons License

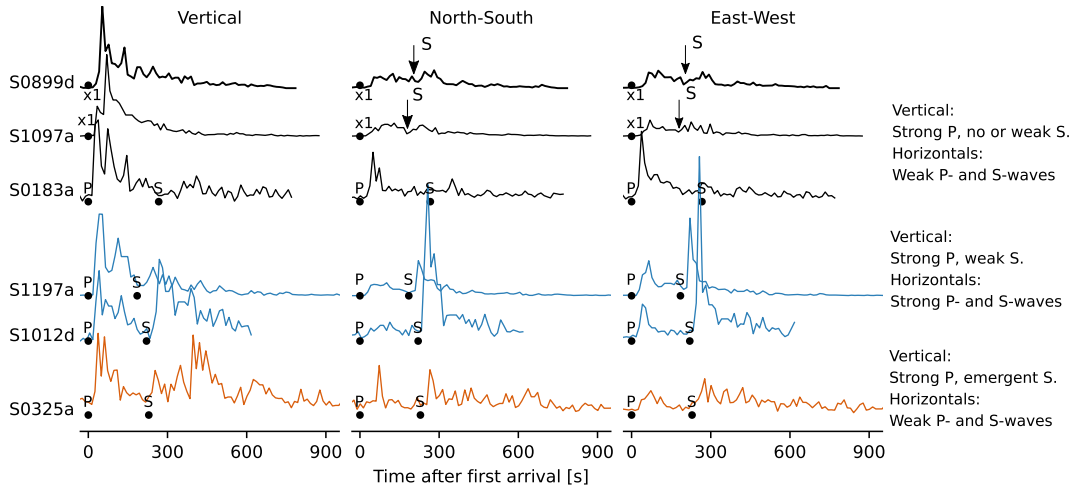

Figure 10. S0899d–like events with three sub-classes. Marsquake Service phase picks are denoted with dots. Only x1 picks were identified for S0899d and S1097a, though frequency-time domain polarization analysis suggests these are P-wave energy. We propose new S-picks for both events using the horizontal components as shown with the down-pointing arrows.

S0183a remains an outlier: Although the event clusters with S0899d in terms of envelope characteristics, its epicenter in the V14 catalog is at a distance of 46° (Figure 6). Khan et al. (2021) provides an alternative distance range and locates S0183a at 54–59° using differential arrival times of seismic phases from multiple events and the current knowledge of mineralogy. Our alignments in Figure 5 favor the solution provided by MQS.

S1012d and S1197a were not assigned a backazimuth in V14. Using the envelope grid search method, we propose that the events have backazimuths of 60 ± 35° and 65 ± 40°, respectively (Figure 11). This means the events locate close to S0325a, so there is now a cluster of three events in this class (Figure 6 and Figure S11 in Supporting Information S1). Due to the 180° ambiguity, it is possible that these events are on the opposite side of the azimuth semicircle. However, the observed seismicity on Mars appears to occur along or north of the equatorial dichotomy (Figure 6); therefore, we find our preferred backazimuth more plausible.

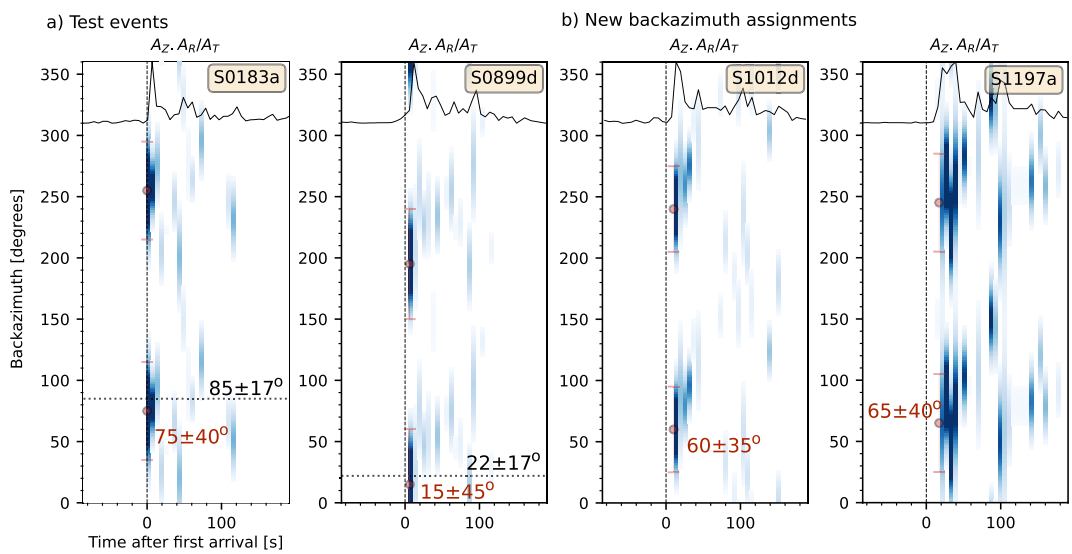

Figure 11. Envelope-based backazimuth estimates for S1012d and S1197a, events at similar distances to S0899d with weak or no S-waves. The dotted horizontal lines in (a) are the backazimuth values reported in the V14 catalog, while orange circles with error bars are our preferred backazimuth estimates. The similarity to the Marsquake Service values from V14 validates the grid search approach. (b) Our new backazimuth estimates for S1012d and S1197a which were reported in the V14 catalog without any values. Other details follow Figure 4.

21699100, 2023, 8, Downloaded from https://agupubs.onlinelibrary.wiley.com/doi/10.1029/2023JE007826 by Cochrane France, Wiley Online Library on [07/09/2023]. See the Terms and Conditions (https://onlinelibrary.wiley.com/terms-and-conditions) on Wiley Online Library for rules of use; OA articles are governed by the applicable Creative Commons License

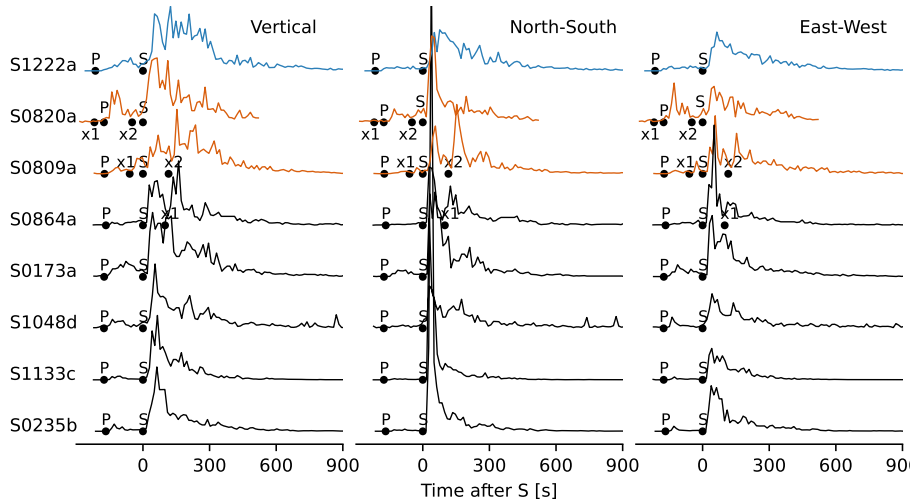

Figure 12. Three-component envelopes for S1222a and a subset of events from the Cerberus Fossae region. The seismic phase picks from V14 are marked with dots. S0820a and S0809a (orange envelopes) are interpreted as event doublets by the Marsquake Service (Ceylan et al., 2022) with the additional phases marked as x1 and x2, instead of P and S, respectively.

The nature of the source behind this event class has yet to be discovered. Giardini et al. (2020) and Khan et al. (2021) explain the lack of S-waves with distance and suggest that S-waves are attenuated between ~40–60° where seismic waves propagate through a low-velocity layer in the upper mantle. With more data available, the epicenters determined by MQS and our re-locations imply a scattered and closer distribution of these events; hence, a single S-wave shadow zone alone cannot explain the lack of S-waves. The low S-wave amplitudes could be caused by geometrical spreading due to strong 3D crustal and mantle structure (Kim, Duran, et al., 2023; Plesa et al., 2022) or the source mechanism, none of which can be confirmed at this time.

3.5. S1222a and the Cerberus Fossae Class

S1222a, which occurred on 4 May 2022, is the largest event (M_W^{Ma}4.6 ± 0.2) recorded since landing; thus, it released a significant part of the total global seismic moment (Knapmeyer et al., 2023). The event is 37° ± 1.6 away from InSight, and unlike most of the LF family, shows clear Rayleigh and Love waves including their overtones (Kim, Stähler, et al., 2023). The backazimuth estimate for S1222a is 101 ± 8° (Kawamura et al., 2023) in the V14 catalog. This places the epicenter NE of Apollinaris Mons, 300–600 km north of the dichotomy boundary (Andrews-Hanna et al., 2008).

Our envelope-based approach presented above obtains 125° ± 15 from the P-wave coda, which is inconsistent with the MQS estimate from the DOP-based method, perhaps due to the emergent character of the body waves. Such a location further south is also suggested by the direction of propagation from the fundamental mode minor-arc surface waves and their overtones (Kim, Stähler, et al., 2023; Panning et al., 2023). This would place the epicenter close to or potentially even south of the Martian dichotomy boundary. Surface wave measurements in the S1222a recording also support a crustal propagation path predominantly in the southern highlands, where thicker crust is expected (Kim, Duran, et al., 2023). Interestingly, although the event did not originate in the CF, its envelopes are largely similar in shape to those from the region (Figures 2 and 12).

InSight did not record any marsquakes closer than 25° from the station (Figure 1a). A large number of the LF-family events, which show relatively clear P- and S-wave arrivals, are located in the CF region, 25–35° away from the station due east (Durán, Khan, Ceylan, Zenhäusern, et al., 2022; Stähler et al., 2022). Within this cluster of events, the decay of P- and S-wave coda is similar, although some events show higher relative energy in their coda (e.g., S0173a vs. S0235b; Figure S9 in Supporting Information S1).

Stähler et al. (2022) attributes the seismicity in the general Cerberus region to the active deformation caused by recent volcanism, and propose the CF as the source. The authors also show that the HF events come from a similar direction as the LF family events located in the region and propose that all HF events originate from the central part of CF in the form of very shallow events associated with the graben flanks. Since the study, four more events

21699100, 2023, 8, Downloaded from https://agupubs.onlinelibrary.wiley.com/doi/10.1029/2023JE007826 by Cochrane France, Wiley Online Library on [07/09/2023]. See the Terms and Conditions (https://onlinelibrary.wiley.com/terms-and-conditions) on Wiley Online Library for rules of use; OA articles are governed by the applicable Creative Commons License

21699100, 2023, 8, Downloaded from https://agupubs.onlinelibrary.wiley.com/doi/10.1029/2023JE007826 by Cochrane France, Wiley Online Library on [07/09/2023]. See the Terms and Conditions (https://onlinelibrary.wiley.com/terms-and-conditions) on Wiley Online Library for rules of use; OA articles are governed by the applicable Creative Commons License

(S1015f, S1022a, S1048d, and S1133c) were recorded with comparable locations in the V14 catalog with Stähler et al. (2022)'s event set.

Considering the backazimuth uncertainties (Figure S12 in Supporting Information S1), it is plausible that CF is the source region for these events, which is also one of the youngest features on the surface of Mars with evidence of recent (53–210 ka) explosive volcanism (Horvath et al., 2021). However, the strike of the CF fault system is directed NW-SE (yellow lines in Figure 6c and Figure S12 in Supporting Information S1), while the epicenters of events attributed to the CF follow an N-S trend. We interpret that this class of events originated from the CF, and project all events in this class to the center of the fault system while maintaining their reported distances in order to be consistent with the surface observations (Knapmeyer et al., 2006; Perrin et al., 2022).

4. Conclusions

We find that over the lifetime of the mission, InSight did not observe a wide distribution of seismicity across the planet, but rather the seismicity is focused in a few distance ranges and locations along or north of the Martian dichotomy (Figure 6). This seems to be mostly in line with pre-mission estimates where seismicity focusing on regions with young surface faulting (Golombek et al., 1992; Knapmeyer et al., 2006; Plesa et al., 2018) was also considered. The many marsquakes in CF and the possible association of marsquakes with extensional faulting near Olympus Mons imply that contraction due to cooling is not the dominant driver of present-day Martian tectonics, as proposed for other smaller terrestrial planets, Mercury and the Moon (Byrne et al., 2014):

1. A number of low SNR events, which are likely distant events due to their very long duration and were originally located by visual alignments at distances >90°, are found to be highly similar to S1000a^{I} at 126° away from InSight. Although we cannot rule out other possible source regions at these distances, in light of the only evidence of seismicity from S0976a, we propose that these events are likely to occur in southern Tharsis region, plausibly in western VM (Figures 6b and 6d). The absence of observed seismicity from the heavily faulted Tharsis region had been puzzling beforehand, but can now be explained by the fact that PP and SS waves from these distances are generally highly scattered (Lognonné et al., 2020; Zenhäusern et al., 2022) and can only be identified as such by comparison to template events such as S1000a^{I}.
2. Two events (S1153a and S1415a) have similar envelope shapes (Figure 8b) and spectral content (Figure S2 in Supporting Information S1). These events have distances around 90° as computed by MQS. We find a backazimuth of 85° for S1153a (Figure 8a), and locate both of these events in the approximate area of Olympus Mons (Figure 6), which is surrounded by a basal scarp of 2–10 km height and thrust faults as young as <40 Ma (Weller, 2015), as well as potential grabens cutting through young, late Amazonian terrain (Hargitai & Gulick, 2018).
3. S0185a and S0234c can be paired with the impact S1094b^{I}. The event distances are compatible with a source region at a distance of ∼60° (Figures 5 and 9); however, since S0185a and S0234c have no convincing indication of backazimuth, we are not able to identify a single source region.
4. A subset of events (S0899d class) show little or no S-wave energy, specifically on the vertical component (Figure 5). We computed backazimuths for two of the events in this class (S1012d, S1197a; Figure 11). This class of events shows no spatial clustering; therefore, the source region is unknown. The lack of stronger S-waves remains puzzling. Possible reasons are source mechanism, geometrical spreading due to strong 3D mantle structure or a relatively thin S-wave low velocity zone due to a velocity inversion in the lithosphere (Khan et al., 2021).
5. Stähler et al. (2022) evaluates 12 of the events we analyzed here to originate in the CF fault system. Considering the location uncertainties (Figure S12 in Supporting Information S1), we find this plausible, and add four more events with similar characteristics which occurred later in the mission. The main seismogenic region on InSight's hemisphere of Mars (Figure 1) remains to be the central part of CF (InSight Marsquake Service, 2023; Stähler et al., 2022), with original MQS epicenters aligned in a N-S trend (Figures 6a and 6c). Since the faults in the region have a strike along NW-SE direction (Perrin et al., 2022), we re-assign those events to the center of the Cerberus Fault system based on our interpretation.

Our re-locations have no effect on the recent interior models from InSight since we do not adjust the locations or seismic phase picks for the high-quality events. However, our re-evaluations of for example, the distant event class, are potentially important for future studies aiming at the deep interior of Mars, as they highlight events in which deep mantle or core-traversing phases could be present. Also, it paves the way for a quantitative analysis of regional and global co-seismic deformation estimates of planet Mars.

Data Availability Statement

The waveform data and seismicity catalog are available from InSight Mars SEIS Data Service (2019a, 2019b). The InSight seismicity catalog is from InSight Marsquake Service (2023). We used the ObsPy (Krischer et al., 2015), NumPy (Harris et al., 2020) and scipy (Virtanen et al., 2020) packages for data processing. We benefited from the tslearn package of Tavenard et al. (2020) for similarity analysis, and Elson et al. (2022) for maps. The python scripts and seismic data used for the similarity analysis can be found in Ceylan et al. (2023).

Acknowledgments
We acknowledge NASA, CNES, partner agencies and institutions (UKSA, SSO, DLR, JPL, IPGP-CNRS, ETHZ, ICL, MPS-MPG), and the operators of JPL, SISMOC, MSDS, IRISDMC and PDS for providing the SEIS data. Marsquake Service operations at ETH are supported by ETH Research Grant ETH-06 17-02. The authors recognize support from the ETH+ funding scheme (ETH+02 19-1: "Planet Mars"). This is InSight Contribution Number 195. Open access funding provided by Eidgenossische Technische Hochschule Zurich.

References

Andrews-Hanna, J. C., Zuber, M. T., & Banerdt, W. B. (2008). The Borealis basin and the origin of the Martian crustal dichotomy. *Nature*, *453*(7199), 1212–1215. https://doi.org/10.1038/nature07011

Banerdt, W. B., Smrekar, S. E., Banfield, D., Giardini, D., Golombek, M., Johnson, C. L., et al. (2020). Initial results from the InSight mission on Mars. *Nature Geoscience*, *13*(3), 183–189. https://doi.org/10.1038/s41561-020-0544-y

Banfield, D., Spiga, A., Newman, C., Forget, F., Lemmon, M., Lorenz, R., et al. (2020). The atmosphere of Mars as observed by InSight. *Nature Geoscience*, *13*(3), 190–198. https://doi.org/10.1038/s41561-020-0534-0

Böse, M., Clinton, J. F., Ceylan, S., Euchner, F., van Driel, M., Khan, A., et al. (2017). A probabilistic framework for single-station location of seismicity on Earth and Mars. *Physics of the Earth and Planetary Interiors*, *262*, 48–65. https://doi.org/10.1016/j.pepi.2016.11.003

Böse, M., Giardini, D., Stähler, S., Ceylan, S., Clinton, J. F., van Driel, M., et al. (2018). Magnitude scales for Marsquakes. *Bulletin of the Seismological Society of America*, *108*(5A), 2764–2777. https://doi.org/10.1785/0120180037

Böse, M., Stähler, S. C., Deichmann, N., Giardini, D., Clinton, J., Lognonné, P., et al. (2021). Magnitude scales for Marsquakes calibrated from InSight data. *Bulletin of the Seismological Society of America*, *111*(6), 3003–3015. https://doi.org/10.1785/0120210045

Byrne, P. K., Klimczak, C., Celâl Şengör, A. M., Solomon, S. C., Watters, T. R., & Hauck, S. A., II. (2014). Mercury's global contraction much greater than earlier estimates. *Nature Geoscience*, *7*(4), 301–307. https://doi.org/10.1038/ngeo2097

Ceylan, S., Clinton, J. F., Giardini, D., Böse, M., Charalambous, C., van Driel, M., et al. (2021). Companion guide to the marsquake catalog from InSight, Sols 0–478: Data content and non-seismic events. *Physics of the Earth and Planetary Interiors*, *310*, 106597. https://doi.org/10.1016/j.pepi.2020.106597

Ceylan, S., Clinton, J. F., Giardini, D., Stähler, S. C., Horleston, A., Kawamura, T., et al. (2022). The Marsquake catalogue from InSight, sols 0–1011. *Physics of the Earth and Planetary Interiors*, *333*, 106943. https://doi.org/10.1016/j.pepi.2022.106943

Ceylan, S., Giardini, D., Clinton, J. F., Kim, D., Khan, A., Stähler, S. C., et al. (2023). Supplement for "Mapping the seismicity of Mars with InSight". Zenodo. https://doi.org/10.5281/zenodo.8079513

Clinton, J., Ceylan, S., van Driel, M., Giardini, D., Stähler, S., Böse, M., et al. (2021). The Marsquake catalogue from InSight, sols 0–478. *Physics of the Earth and Planetary Interiors*, *310*, 106595. https://doi.org/10.1016/j.pepi.2020.106595

Clinton, J., Giardini, D., Böse, M., Ceylan, S., van Driel, M., Euchner, F., et al. (2018). The Marsquake service: Securing daily analysis of SEIS data and building the Martian seismicity catalogue for InSight. *Space Science Reviews*, *214*(8), 133. https://doi.org/10.1007/s11214-018-0567-5

Coles, K. S., Tanaka, K. L., & Christensen, P. R. (2019). *The Atlas of Mars: Mapping its Geography and Geology*. Cambridge University Press. https://doi.org/10.1017/9781139567428

Daubar, I., Fernando, B., Garcia, R., Peter, G., Zenhaeusern, G., Wójcicka, N., et al. (2023). Two seismic events from InSight confirmed as new impacts on Mars. EarthArXiv. https://doi.org/10.31223/x5894h

Drilleau, M., Samuel, H., Garcia, R. F., Rivoldini, A., Perrin, C., Michaut, C., et al. (2022). Marsquake locations and 1-D seismic models for Mars from InSight data. *Journal of Geophysical Research: Planets*, *127*(9), e2021JE007067. https://doi.org/10.1029/2021JE007067

Durán, C., Khan, A., Ceylan, S., Charalambous, C., Kim, D., Drilleau, M., et al. (2022). Observation of a core-diffracted P-wave from a farside impact with implications for the lower-mantle structure of Mars. *Geophysical Research Letters*, *49*(21), e2022GL100887. https://doi.org/10.1029/2022GL100887

Durán, C., Khan, A., Ceylan, S., Zenhäusern, G., Stähler, S., Clinton, J., & Giardini, D. (2022). Seismology on Mars: An analysis of direct, reflected, and converted seismic body waves with implications for interior structure. *Physics of the Earth and Planetary Interiors*, *325*, 106851. https://doi.org/10.1016/j.pepi.2022.106851

Elson, P., de Andrade, E. S., Lucas, G., May, R., Hattersley, R., Campbell, E., et al. (2022). Scitools/cartopy: V0.21.1. Zenodo. https://doi.org/10.5281/zenodo.7430317

Garcia, R. F., Daubar, I. J., Beucler, É., Posiolova, L. V., Collins, G. S., Lognonné, P., et al. (2022). Newly formed craters on mars located using seismic and acoustic wave data from insight. *Nature Geoscience*, *15*(10), 774–780. https://doi.org/10.1038/s41561-022-01014-0

Giardini, D., Lognonné, P., Banerdt, W. B., Pike, W. T., Christensen, U., Ceylan, S., et al. (2020). The seismicity of Mars. *Nature Geoscience*, *13*(3), 205–212. https://doi.org/10.1038/s41561-020-0539-8

Golombek, M. P., Banerdt, W. B., Tanaka, K. L., & Tralli, D. M. (1992). A prediction of Mars seismicity from surface faulting. *Science*, *258*(5084), 979–981. https://doi.org/10.1126/science.258.5084.979

Gudkova, T. V., Batov, A. V., & Zharkov, V. N. (2017). Model estimates of non-hydrostatic stresses in the Martian crust and mantle: 1—Two-level model. *Solar System Research*, *51*(6), 457–478. https://doi.org/10.1134/S003809461706003X

Hargitai, H. I., & Gulick, V. C. (2018). Late Amazonian–Aged channel and island systems located East of Olympus Mons, Mars. In R. J. Soare, S. J. Conway, & S. M. Clifford (Eds.), *Dynamic Mars* (pp. 121–154). Elsevier. https://doi.org/10.1016/B978-0-12-813018-6.00004-2

Harris, C. R., Millman, K. J., van der Walt, S. J., Gommers, R., Virtanen, P., Cournapeau, D., et al. (2020). Array programming with NumPy. *Nature*, *585*(7825), 357–362. https://doi.org/10.1038/s41586-020-2649-2

Horleston, A., Clinton, J., Ceylan, S., Giardini, D., Charalambous, C., Irving, J., et al. (2022). The far side of Mars: Two distant marsquakes detected by InSight. *The Seismic Record*, *2*(2), 88–99. https://doi.org/10.1785/0320220007

Horvath, D. G., Moitra, P., Hamilton, C. W., Craddock, R. A., & Andrews-Hanna, J. C. (2021). Evidence for geologically recent explosive volcanism in Elysium Planitia, Mars. *Icarus*, *365*, 114499. https://doi.org/10.1016/j.icarus.2021.114499

InSight Marsquake Service. (2020). *Mars Seismic Catalogue, InSight Mission; V3 2020-07-01*. ETHZ, IPGP, JPL, ICL, ISAE-Supaero, MPS, University of Bristol. https://doi.org/10.12686/a8

InSight Marsquake Service. (2022). *Mars Seismic Catalogue, InSight Mission; V12 2022-10-01*. ETHZ, IPGP, JPL, ICL, University of Bristol. https://doi.org/10.12686/a18

21699100, 2023, 8, Downloaded from https://agupubs.onlinelibrary.wiley.com/doi/10.1029/2023JE007826 by Cochrane France, Wiley Online Library on [07/09/2023]. See the Terms and Conditions (https://onlinelibrary.wiley.com/terms-and-conditions) on Wiley Online Library for rules of use; OA articles are governed by the applicable Creative Commons License

InSight Marsquake Service. (2023). *Mars Seismic Catalogue, InSight Mission; V14 2023-04-01*. ETHZ, IPGP, JPL, ICL, University of Bristol. https://doi.org/10.12686/a21

InSight Mars SEIS Data Service. (2019a). InSight SEIS data bundle. *PDS Geosciences (GEO) Node*. https://doi.org/10.17189/1517570

InSight Mars SEIS Data Service. (2019b). *SEIS raw data, Insight Mission*. IPGP, JPL, CNES, ETHZ, ICL, MPS, ISAE-Supaero, LPG, MFSC. https://doi.org/10.18715/SEIS.INSIGHT.XB_2016

Irving, J. C. E., Lekić, V., Durán, C., Drilleau, M., Kim, D., Rivoldini, A., et al. (2023). First observations of core-transiting seismic phases on Mars. *Proceedings of the National Academy of Sciences*, *120*(18), e2217090120. https://doi.org/10.1073/pnas.2217090120

Kawamura, T., Clinton, J. F., Zenhausern, G., Ceylan, S., Horleston, A. C., Dahmen, N. L., et al. (2023). S1222a - The largest Marsquake detected by insight. *Geophysical Research Letters*, *50*(5), e2022GL101543. https://doi.org/10.1029/2022GL101543

Kedar, S., Panning, M. P., Smrekar, S. E., Stähler, S. C., King, S. D., Golombek, M. P., et al. (2021). Analyzing low frequency seismic events at Cerberus Fossae as long period volcanic quakes. *Journal of Geophysical Research: Planets*, *126*(4), e2020JE006518. https://doi.org/10.1029/2020JE006518

Khan, A., Ceylan, S., van Driel, M., Giardini, D., Lognonné, P., Samuel, H., et al. (2021). Upper mantle structure of Mars from InSight seismic data. *Science*, *373*(6553), 434–438. https://doi.org/10.1126/science.abf2966

Khan, A., van Driel, M., Böse, M., Giardini, D., Ceylan, S., Yan, J., et al. (2016). Single-station and single-event marsquake location and inversion for structure using synthetic Martian waveforms. *Physics of the Earth and Planetary Interiors*, *258*, 28–42. https://doi.org/10.1016/j.pepi.2016.05.017

Kim, D., Banerdt, W., Ceylan, S., Giardini, D., Lekić, V., Lognonné, P., et al. (2022). Surface waves and crustal structure on Mars. *Science*, *378*(6618), 417–421. https://doi.org/10.1126/science.abq7157

Kim, D., Davis, P., Lekić, V., Maguire, R., Compaire, N., Schimmel, M., et al. (2021). Potential pitfalls in the analysis and structural interpretation of seismic data from the Mars InSight mission. *Bulletin of the Seismological Society of America*, *111*(6), 2982–3002. https://doi.org/10.1785/0120210123

Kim, D., Duran, C., Giardini, D., Plesa, A.-C., Stähler, S. C., Boehm, C., et al. (2023). Global crustal thickness revealed by surface waves orbiting Mars. *Geophysical Research Letters*, *50*(12), e2023GL103482. https://doi.org/10.1029/2023GL103482

Kim, D., Stähler, S., Ceylan, S., Lekic, V., Maguire, R., Zenhäusern, G., et al. (2023). Structure along the Martian dichotomy constrained by Rayleigh and love waves and their overtones. *Geophysical Research Letters*, *50*(8), e2022GL101666. https://doi.org/10.1029/2022GL101666

Knapmeyer, M., Oberst, J., Hauber, E., Wählisch, M., Deuchler, C., & Wagner, R. (2006). Working models for spatial distribution and level of Mars' seismicity. *Journal of Geophysical Research*, *111*(E11), E11006. https://doi.org/10.1029/2006JE002708

Knapmeyer, M., Stähler, S., Plesa, A.-C., Ceylan, S., Charalambous, C., Clinton, J., et al. (2023). The global seismic moment rate of Mars after event S1222a. *Geophysical Research Letters*, *50*(7), e2022GL102296. https://doi.org/10.1029/2022GL102296

Krischer, L., Megies, T., Barsch, R., Beyreuther, M., Lecocq, T., Caudron, C., & Wassermann, J. (2015). ObsPy: A bridge for seismology into the scientific Python ecosystem. *Computational Science & Discovery*, *8*(1), 014003. https://doi.org/10.1088/1749-4699/8/1/014003

Lognonné, P., Banerdt, W., Giardini, D., Pike, W., Christensen, U., Laudet, P., et al. (2019). SEIS: Insight's seismic experiment for internal structure of Mars. *Space Science Reviews*, *215*(1), 12. https://doi.org/10.1007/s11214-018-0574-6

Lognonné, P., Banerdt, W., Pike, W., Giardini, D., Christensen, U., Garcia, R., et al. (2020). Constraints on the shallow elastic and anelastic structure of Mars from InSight seismic data. *Nature Geoscience*, *13*(3), 213–220. https://doi.org/10.1038/s41561-020-0536-y

Panning, M. P., Banerdt, W. B., Beghein, C., Carrasco, S., Ceylan, S., Clinton, J. F., et al. (2023). Locating the largest event observed on mars with multi-orbit surface waves. *Geophysical Research Letters*, *50*(1), e2022GL101270. https://doi.org/10.1029/2022GL101270

Perrin, C., Jacob, A., Lucas, A., Myhill, R., Hauber, E., Batov, A., et al. (2022). Geometry and segmentation of Cerberus Fossae, Mars: Implications for marsquake properties. *Journal of Geophysical Research: Planets*, *127*(1), e2021JE007118. https://doi.org/10.1029/2021JE007118

Plesa, A.-C., Knapmeyer, M., Golombek, M. P., Breuer, D., Grott, M., Kawamura, T., et al. (2018). Present-day Mars' seismicity predicted from 3-D thermal evolution models of interior dynamics. *Geophysical Research Letters*, *45*(6), 2580–2589. https://doi.org/10.1002/2017GL076124

Plesa, A.-C., Wieczorek, M., Knapmeyer, M., Rivoldini, A., Walterová, M., & Breuer, D. (2022). Interior dynamics and thermal evolution of Mars – A geodynamic perspective. In *Advances in Geophysics* (Vol. 63, pp. 179–230). Elsevier. https://doi.org/10.1016/bs.agph.2022.07.005

Posiolova, L. V., Lognonné, P., Banerdt, W. B., Clinton, J., Collins, G. S., Kawamura, T., et al. (2022). Largest recent impact craters on Mars: Orbital imaging and surface seismic co-investigation. *Science*, *378*(6618), 412–417. https://doi.org/10.1126/science.abq7704

Sakoe, H., & Chiba, S. (1978). Dynamic programming algorithm optimization for spoken word recognition. *IEEE Transactions on Acoustics, Speech, and Signal Processing*, *26*(1), 43–49. https://doi.org/10.1109/TASSP.1978.1163055

Schimmel, M., & Gallart, J. (2004). Degree of polarization filter for frequency-dependent signal enhancement through noise suppression. *Bulletin of the Seismological Society of America*, *94*(3), 1016–1035. https://doi.org/10.1785/0120030178

Scholz, J.-R., Widmer-Schnidrig, R., Davis, P., Lognonné, P., Pinot, B., Garcia, R. F., et al. (2020). Detection, analysis, and removal of glitches from InSight's seismic data from Mars. *Earth and Space Science*, *7*(11), e2020EA001317. https://doi.org/10.1029/2020EA001317

Senthil Kumar, P., Krishna, N., Prasanna Lakshmi, K., Raghukanth, S., Dhabu, A., & Platz, T. (2019). Recent seismicity in Valles Marineris, Mars: Insights from young faults, landslides, boulder falls and possible mud volcanoes. *Earth and Planetary Science Letters*, *505*, 51–64. https://doi.org/10.1016/j.epsl.2018.10.008

Smith, D. E., Zuber, M. T., Frey, H. V., Garvin, J. B., Head, J. W., Muhleman, D. O., et al. (2001). Mars Orbiter Laser Altimeter: Experiment summary after the first year of global mapping of Mars. *Journal of Geophysical Research*, *106*(E10), 23689–23722. https://doi.org/10.1029/2000JE001364

Spohn, T., Hudson, T. L., Witte, L., Wippermann, T., Wisniewski, L., Kedziora, B., et al. (2022). The InSight-HP3 mole on Mars: Lessons learned from attempts to penetrate to depth in the Martian soil. *Advances in Space Research*, *69*(8), 3140–3163. https://doi.org/10.1016/j.asr.2022.02.009

Stähler, S. C., Khan, A., Banerdt, W. B., Lognonné, P., Giardini, D., Ceylan, S., et al. (2021). Seismic detection of the Martian core. *Science*, *373*(6553), 443–448. https://doi.org/10.1126/science.abi7730

Stähler, S. C., Mittelholz, A., Perrin, C., Kawamura, T., Kim, D., Knapmeyer, M., et al. (2022). Tectonics of Cerberus Fossae unveiled by marsquakes. *Nature Astronomy*, *6*(12), 1376–1386. https://doi.org/10.1038/s41550-022-01803-y

Tavenard, R., Faouzi, J., Vandewiele, G., Divo, F., Androz, G., Holtz, C., et al. (2020). Tslearn, a machine learning toolkit for time series data. *Journal of Machine Learning Research*, *21*(118), 1–6.

Tenzer, R., Eshagh, M., & Jin, S. (2015). Martian sub-crustal stress from gravity and topographic models. *Earth and Planetary Science Letters*, *425*, 84–92. https://doi.org/10.1016/j.epsl.2015.05.049

Virtanen, P., Gommers, R., Oliphant, T. E., Haberland, M., Reddy, T., Cournapeau, D., et al. (2020). SciPy 1.0: Fundamental algorithms for scientific computing in Python. *Nature Methods*, *17*(3), 261–272. https://doi.org/10.1038/s41592-019-0686-2

Weller, M. B. (2015). Basal Scarp (Olympus Mons, Mars). In H. Hargitai & Á. Kereszturi (Eds.), *Encyclopedia of Planetary Landforms* (pp. 137–141). Springer. https://doi.org/10.1007/978-1-4614-3134-3_14

21699100, 2023, 8, Downloaded from https://agupubs.onlinelibrary.wiley.com/doi/10.1029/2023JE007826 by Cochrane France, Wiley Online Library on [07/09/2023]. See the Terms and Conditions (https://onlinelibrary.wiley.com/terms-and-conditions) on Wiley Online Library for rules of use; OA articles are governed by the applicable Creative Commons License

Zenhäusern, G., Stähler, S. C., Clinton, J. F., Giardini, D., Ceylan, S., & Garcia, R. F. (2022). Low-frequency marsquakes and where to find them: Back azimuth determination using a polarization analysis approach. *Bulletin of the Seismological Society of America*, *112*(4), 1787–1805. https://doi.org/10.1785/0120220019

Zweifel, P., Mance, D., ten Pierick, J., Giardini, D., Schmelzbach, C., Haag, T., et al. (2021). Seismic high-resolution acquisition electronics for the NASA InSight Mission on Mars. *Bulletin of the Seismological Society of America*, *111*(6), 2909–2923. https://doi.org/10.1785/0120210071

21699100, 2023, 8, Downloaded from https://agupubs.onlinelibrary.wiley.com/doi/10.1029/2023JE007826 by Cochrane France, Wiley Online Library on [07/09/2023]. See the Terms and Conditions (https://onlinelibrary.wiley.com/terms-and-conditions) on Wiley Online Library for rules of use; OA articles are governed by the applicable Creative Commons License